Non-square rectangular pile arrangements and load distribution in basal reinforced piled embankments

S.J.M. van Eekelen
Deltares, Delft, Netherlands (Suzanne.vaneekelen@deltares.nl)

H.J. Lodder
RPS Group Plc, Delft, The Netherlands (hermanjaap.lodder@rps.nl)

ABSTRACT: In design rules for the basal geosynthetic reinforcement (GR) of a piled embankment, the GR strips between each pair of adjacent pile caps are assumed to attract most load. Van Eekelen et al., (2015) and Zaeske (2001) showed that this is a realistic assumption. This paper analysis two aspects of the load distribution on these GR strips: (1) how to distribute the load between the transverse and longitudinal GR strips for non-square rectangular pile patterns and (2) how to further distribute the load on each GR strips between a pair of adjacent piles.

In a piled embankment with a non-square rectangular pile pattern, Zaeske (2001) requires least reinforcement in the direction with the largest pile spacing. The Concentric Arches model of Van Eekelen et al. (2013, 2015) requires most reinforcement in that direction with the largest pile spacing. The last one seems a better approach.

Van Eekelen et al., (2015) showed that when there is no subsoil support, or almost no subsoil support, the inverse triangular load distribution on the GR strips gives the best match with a large number of measurements. However, this load distribution is a schematization of the real load distribution that is probably more parabola-like and does not have a zero central point. This paper compares the inverse triangular load distribution with these alternative load distributions and concludes that the difference is very limited. Therefore, the relatively simple inverse triangular load distribution is sufficiently adequate for the situation without or nearly no subsoil support.

Keywords: basal reinforced piled embankments, Concentric Arches model, load-deflection behaviour, non-square rectangular pile patterns, load distribution.

1 INTRODUCTION

Suppose one has designed a square pile pattern for a basal reinforced piled embankment. Local circumstances however, ask for a bit more pile spacing in one direction. The calculations for the geosynthetic reinforcement (GR) are repeated for the larger pile spacing in one direction, and guess what: less GR is needed in the direction that the pile spacing is increased in comparison to the other direction! The designer came across a mistake in the rules of EBGEO (2010) and CUR (2010) and has a difficult job to convince the principle that the design rules cannot be correct and that increasing the pile spacing means increasing the necessary GR tensile strength, in contrary to the EBGEO rules.

This paper gives an explanation for this behaviour of the method of Zaeske (2001), that was adopted in EBGEO (2010) and CUR (2010).

In most calculation models for the design of the basal reinforcement in a piled embankment, the load on the geosynthetic reinforcement is assumed to be concentrated on the GR strips between each pair of adjacent pile caps. Van Eekelen (2015) explains that this is because the GR strips between adjacent piles behave relatively stiffly because the span between adjacent piles is relatively small. Consequently, the GR strips behave more stiffly than the surrounding GR and the GR strips therefore attract much more load than the surrounding GR. This load concentration on the GR strips was measured by Zaeske (2001, see Figure 4.6) and proven with 3D numerical calculations (Van der Peet and Van Eekelen, 2014). This effect is clearest in the cases with little or no subsoil support.

After explaining some basics about basal reinforced piled embankments design in Chapter 2, this paper considers two aspects of the load distribution on the GR strips: (1) how to distribute the load between the transverse and longitudinal GR strips for non-square rectangular pile patterns, which is done in Chapter 4 and (2) how to further distribute the load on each GR strips between a pair of adjacent piles, which is done in Chapter 5.

2 DESIGING THE BASAL REINFORCEMENT OF A PILED EMBANKMENT

2.1 *Two Calculation Steps*

A basal reinforced piled embankment consists of a reinforced embankment on a pile foundation. The reinforcement consists of one or more horizontal layers of geosynthetic reinforcement (GR) installed at the base of the embankment. The design of the GR is the issue considered in this paper. All analytical design models calculate the tensile strain and –force in the GR. The long-term tensile strength of the GR needs to be higher than this tensile force and the GR strains may not exceed acceptable deformation boundaries. The calculation of the GR strain and tensile force includes two calculation steps, as shown in Figure 1 and explained before in for example Van Eekelen (2015).

2.2 *Step 1: Arching*

Calculation step 1 divides the load – the weight of the embankment fill, road construction and traffic load – into two parts: load part *A* (kN/pile) and the 'residual load' (*B*+*C* in kN/pile in Figure 1), which rests on the GR (*B*) and the underlying subsoil (*C*).
Load part *A*, which is also referred to as 'arching *A*', is the part of the load that is transferred to the piles directly. The value of *A* is relatively large due to the arching behaviour in the fill. This arching is the mechanism by which stiffer construction elements attract a large proportion of the load and this is the basis for the GR design. Different analytical models exist to describe this arching behaviour. As this arching model is not the subject of the present study,

all calculations in this paper have been made with the same arching model, namely the Concentric Arches (CA) model of van Eekelen et al., (2012b, 2013, 2015) and van Eekelen (2015).

2.3 *Step 2: Load-Deflection Behaviour of the GR*

Calculation step 2 calculates the GR strain from the residual load *B+C*, which was calculated in step 1. This calculation step considers the load-deflection behaviour of the GR strips between each pair of adjacent piles. Load part *B+C* is assumed to be concentrated on these GR strips. If the piles are arranged in a square pattern, each GR attract the same amount of load. If the piles are arranged in a non-square rectangular pattern, different methods are in use to distribute *B+C* on the transverse and longitudinal GR strips. This is considered in Chapter 4. The GR strips are thus loaded by *B+C* and may or may not be supported by springs that simulate subsoil support. Analysis of this system, shown in Figure 1b, leads to differential equations which can be solved to calculate the GR strain. This is shown in Van Eekelen et al., (2015) and Van Eekelen (2015).

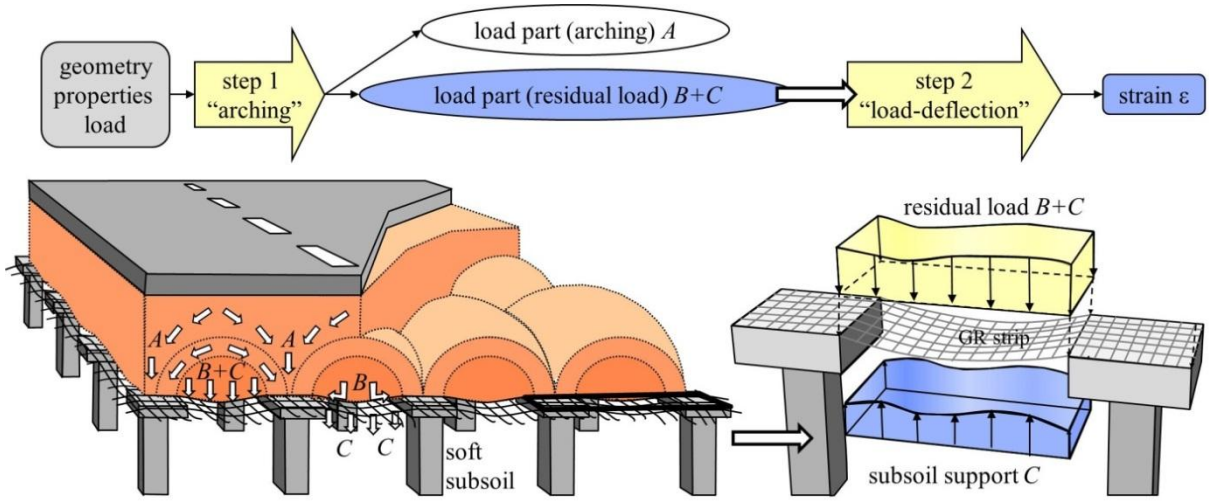

a. Calculation step 1 *b.* Calculation step 2

Figure 1: Calculating the geosynthetic reinforcement (GR) strain comprises two calculation steps.

The GR strain can be calculated if three aspects are know: the distribution of load part *B+C* on a GR strip, which is considered in Chapter 5, the amount of subsoil support and the GR stiffness.

3 INPUT GEOMETRY AND PROPERTIES AND RESULT STEP 1.

Figure 2 and Table 1 introduce the geometry and properties of a case that is used for the calculations in this paper. The pile spacing in the *y*-direction is kept constant at s_y = 2.0 m, the pile spacing s_x in the *x*-direction s_x is also 2.0 m or is varied.

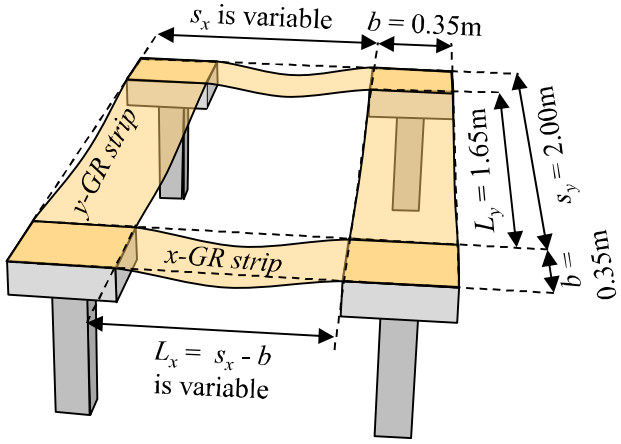

Figure 2: geometry of a non-square rectangular pile arrangement

In this paper, the value of load resting on the GR, *B+C*, is calculated using the Concentric Arches model. The calculated result is given in Table 1 and Figure 3. The next section shows how this load is divided between the GR strips in the transverse and longitudinal directions: the *x*-GR strip and *y*- GR strip as indicated in Figure 2.

Table 1. Geometry and material properties adopted in the calculations of this paper

Property		Unit	
Calculation step 1			
Pile spacing (centre – to – centre distance)	in *x*-direction s_x	m	variable
	in *y*-direction s_y	m	2.00
Width pile cap *b*		m	0.35
Height embankment *H*		m	2.60
Surcharge load *p*		kPa	0
Fill unit weight γ		kN/m^3	18.3
Fill friction angle φ		deg	51
Calculation result for CA model for s_x = s_y = 2.0 m	total load per pile unit $s_x \cdot s_y$	kN/pile	190
	load part *B+C*	kN/pile	65
Calculation result for CA model for s_x = 1.0 m and s_y = 2.0 m	total load per pile unit $s_x \cdot s_y$	kN/pile	96
	load part *B+C*	kN/pile	27
Calculation step 2			
GR stiffness *J*		kN/m	5000
Subgrade reaction *k*		kN/m^3	variable

All calculations presented in this paper were conducted without partial safety factors or model factors.

4 STEP 2A LOAD DISTRIBUTION ON THE TRANSVERSE AND LONGITUDINAL GR STRIPS IN NON-SQUARE RECTANGULAR PILE ARRANGEMENTS

Once the total load resting on the GR, $B+C$, has been calculated, this $B+C$ needs to be distributed over the GR strips in transverse and longitudinal direction. This is done differently in the two models considered here:

- the Zaeske (2001) model, adopted in EBGEO (2010) and CUR (2010) and
- the CA model (Van Eekelen et al., 2015), which is adopted in CUR226 (2016).

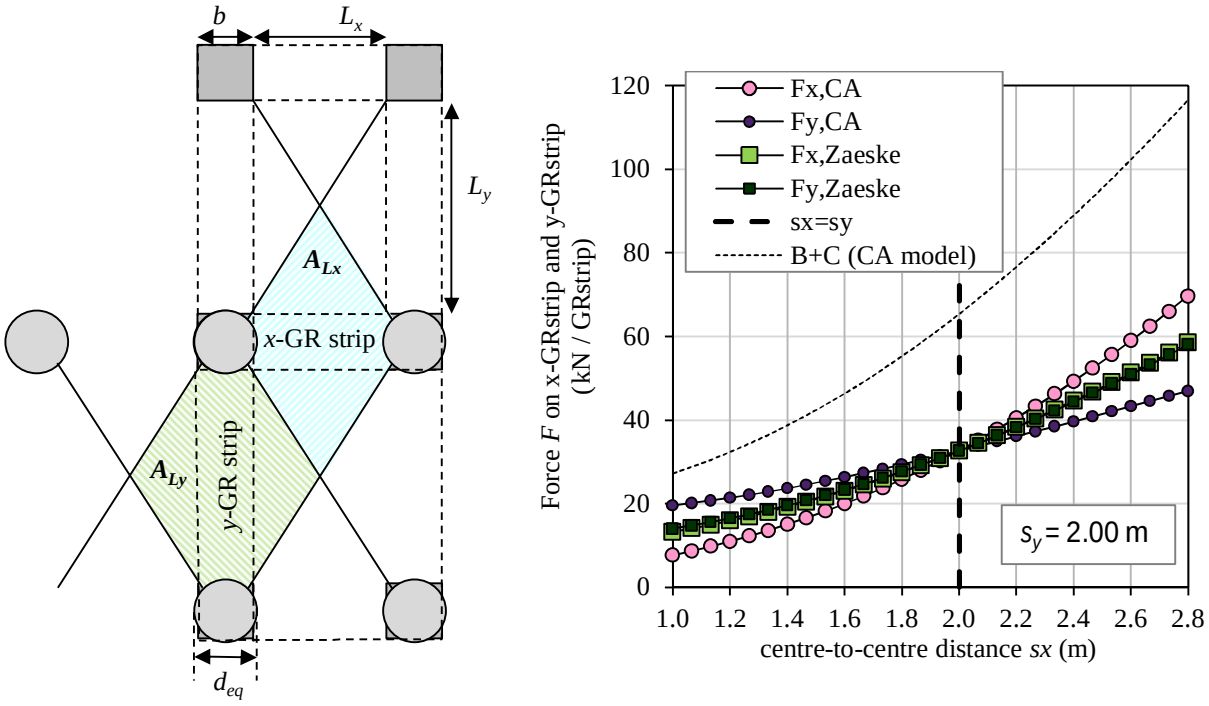

a. rectangular pile pattern *b. distribution of the load between x- and y-GR strips*

Figure 3: Distribution of load $B+C$ between x- and y-GR strips, following the CA model of Van Eekelen et al., (2013, 2015, evenly distributed) and Zaeske (2001) (equivalent to areas-of-diamonds). The load part $B+C$ in these calculations is the same for the CA and the Zaeske calculations in this figure.
For $s_x = s_y = 2.0$ m: $B+C$ =65 kN/pile as given in Table 1. Drawing modified after van Eekelen (2015).

If $s_x = s_y$, there is no difference between the two methods. If $s_x \neq s_y$, however, the two methods give different results. The two methods distribute load part $B+C$ as follows over the transverse and longitudinal GR strips:

4.1 *Distribution of B+C over the transverse and longitudinal GR strips with Zaeske (2001)*

Zaeske (2001) determines the average load on the total GR area between the piles as:

$$\sigma_{v;GR} = \frac{B+C}{s_x \cdot s_y - A_{pile\ cap}} \tag{1}$$

This average pressure on the GR is multiplied with the diamond areas belonging to each GR strip to get the vertical force $F_{x,Z}$ in kN on the x-GR strip and $F_{y,Z}$ on the y-GR strip respectively:

$$F_{x,Z} = \sigma_{v;GR} \cdot A_{Lx} \qquad F_{y,Z} = \sigma_{v;GR} \cdot A_{Ly} \tag{2}$$

Where: A_{Lx} and A_{Ly} in m^2 are the areas of the diamond areas indicated in Figure 3:

$$A_{Lx} = \tfrac{1}{2} \cdot \left(s_x \cdot s_y \right) - \frac{d^2}{2} \cdot \arctan\left(\frac{s_y}{s_x} \right)$$
$$A_{Ly} = \tfrac{1}{2} \cdot \left(s_x \cdot s_y \right) - \frac{d^2}{2} \cdot \arctan\left(\frac{s_x}{s_y} \right) \qquad (3)$$

Where the arctan should be calculated in radians. The forces $F_{x,Z}$ and $F_{y,Z}$ are distributed over the strips in calculation step 2, as discussed in Section 5. The average stress $q_{av,Z}$ in kPa on each GR strip according to Zaeske is:

$$q_{av,x,Z} = F_{x;Z} \cdot A_{x-GRstrip} \qquad q_{av,y,Z} = F_{y;Z} \cdot A_{y-GRstrip} \qquad (4)$$

where $A_{x\text{-}strip}$ and $A_{y\text{-}strip}$ are the areas of the *x*-GR strip and *y*-GR strip respectively.

4.2 *Distribution of B+C over the transverse and longitudinal GR strips with the CA model*

In the case of the Concentric Arches (CA) model, the load $B+C$ in kN/pile on the GR is distributed equally over the area of the GR strips, so that the average load in kPa on the strips is:

$$q_{av;CA} = \frac{B+C}{A_{x-GRstrip} + A_{y-GRstrip}} \qquad (5)$$

This load may be distributed differently than uniformly as discussed in Section 5. The vertical forces $F_{x,CA}$ and $F_{y,CA}$ on the *x*-GR strips and the *y*-GR strips are respectively:

$$F_{x,CA} = q_{av} \cdot L_x \cdot b \qquad F_{y,CA} = q_{av} \cdot L_y \cdot b \qquad (6)$$

where L_x, L_y and b (m) are indicated in Figure 3*a*.

4.3 *Comparison*

Figure 3*b* shows the resulting force on the GR strips for the two methods. In the figure, the centre-to-centre distance s_y is kept constant and s_x is varied. The load distribution between the GR strips is the same for both models for $s_x = s_y = 2.00$ m. The Zaeske model approximately gives the same load in kN/GRstrip in both directions. The CA model gives more load in kN/GRstrip on the longer GR strips than on the shorter GR strips. However, the distributed stress in kPa on the GR strips is the same for the CA in both directions, but different for the Zaeske model, as shown in Figure 4 for $s_x = 1.00$ m and $s_y = 2.00$ m.

The necessary GR strength following from the ultimate limit state (ULS) calculations is linearly related to the calculated GR strainε_{GR} as the GR tensile force is $J \cdot \varepsilon_{GR}$. The implication of the difference in load distribution on the GR strain ε_{GR} and therefore the necessary GR strength is shown in Figure 5: if $s_x < s_y$:

- The CA model gives $\varepsilon_x < \varepsilon_y$, which seems realistic: a higher GR strength, thus more reinforcement is needed in the direction with the largest pile spacing and less reinforcement is needed in the direction with the smallest pile spacing.
- Zaeske gives $\varepsilon_x \approx \varepsilon_y$ for the case without subsoil support (Figure 5*a*) and $\varepsilon_x < \varepsilon_y$. for the case with subsoil support (Figure 5*b*). This does not seem realistic: less GR is needed in the direction with the largest pile spacing than in the direction with smallest pile spacing.

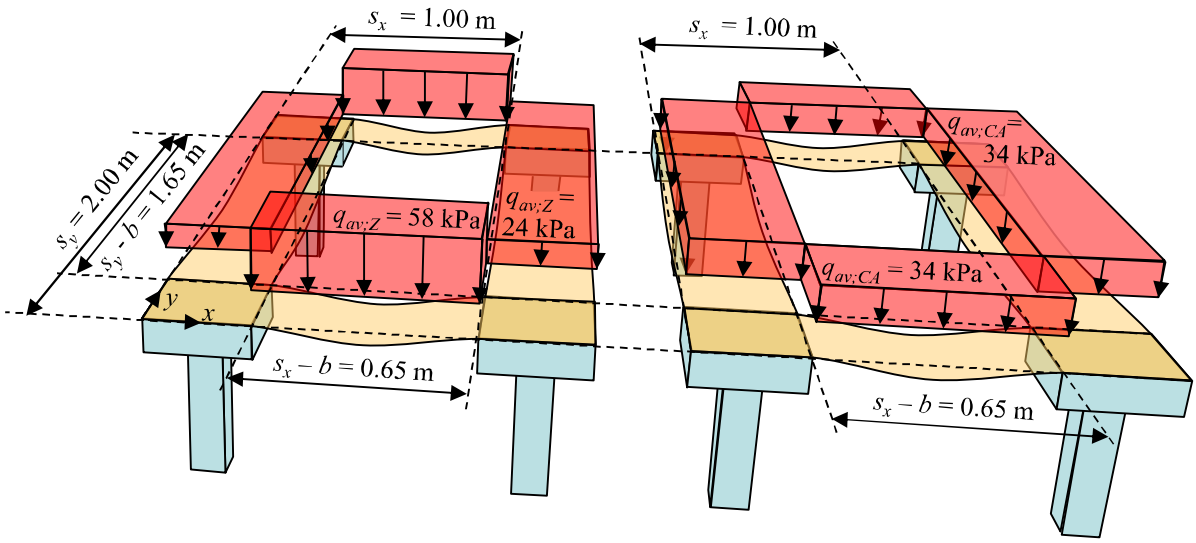

a. Zaeske's (2001) diamond-area-related load distribution

b. Concentric Arches model (van Eekelen et al., 2013); load distributed uniformly over the GR strips

Figure 4: 3D visualisation of the distribution of the load between transverse and longitudinal GR strips: average load on each GR strip. Piles spacing: s_x = 1.0 m and s_y = 2.0 m. Load part *B*+*C* on the GR in these calculations is 27 kN/pile per pile unit (per 1 *x*-GR strip and 1 *y*-GR strip, as given in Table 1).

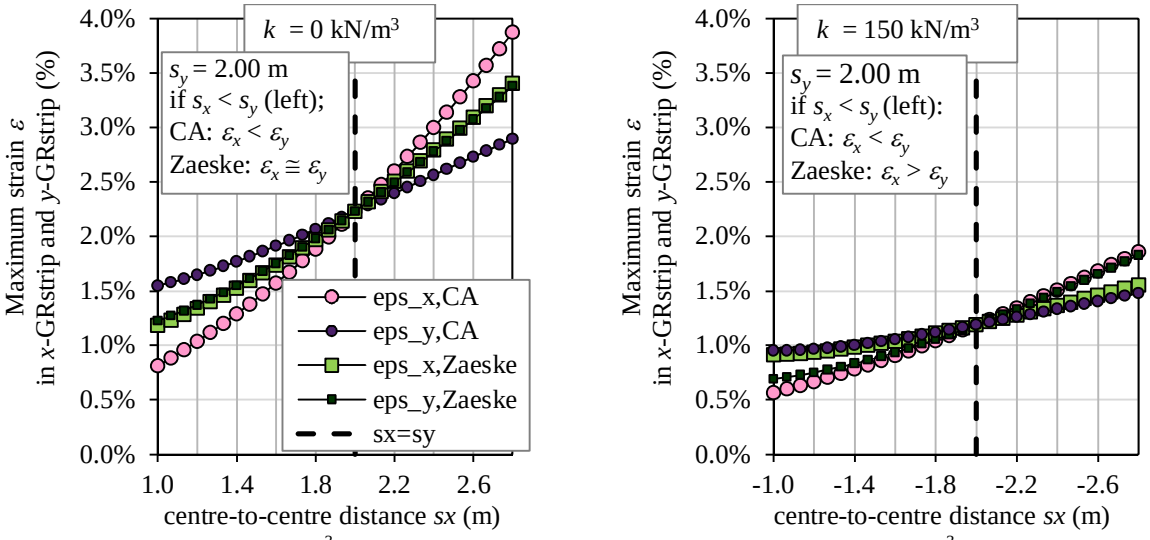

a. No subsoil (k=0 kN/m^3)

b. Subsoil (k = 150 kN/m^3)

Figure 5: Max GR strain in *x*- and *y*-GR strips based on the GR strip forces in Figure 3. The pile spacing in the *y*-direction is s_y = 2.00 m, so, *B*+*C* = 65 kN/pile for all calculations in this figure. Table 1 gives the other input parameters. The strains were calculated with the inverse triangular load distribution and 'all subsoil' (van Eekelen et al, 2015). All calculations were the same except that they used the results given in Figure 3b. All load distribution patterns (Chapter 5) gives the same tendencies. Drawing modified after van Eekelen (2015).

Frequently, principles require a maximum GR strain in the serviceability limit state (SLS). In that case, the resulting necessary GR strength (or GR stiffness) is also linearly related to the calculated the GR strainε, so the conclusions above are also true for this case. The maximum GR deflection might also be normative in design. In that case, the calculated necessary GR stiffness or strength is related to the calculated maximum GR deflection, which is shown in Figure 6. To check differential settlements at ground surface, numerical calculations are needed in addition to the analytical calculations (CUR226, 2016).

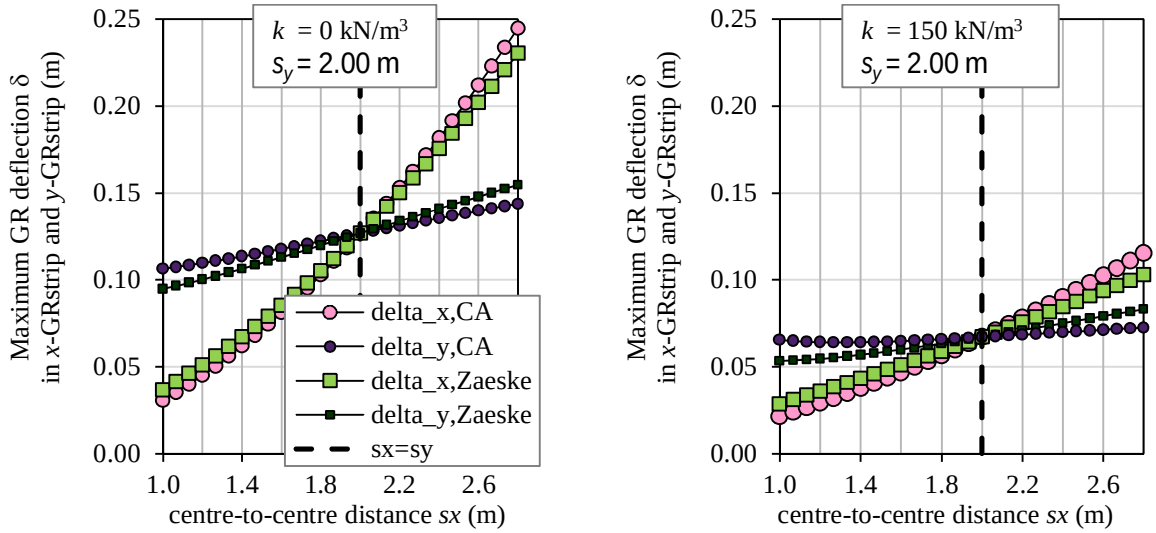

a. No subsoil (k=0 kN/m³) *b. Subsoil (k = 150 kN/m³)*

Figure 6: Maximum GR deflection in *x*- and *y*-GR strips based on the GR strip forces in Figure 3. The calculations were the same as in Figure 5.

5 LOAD DISTRIBUTION ON GR STRIPS

The load distribution on the GR strips depends on the GR deflection. The areas with the least GR deflection attract most load. The GR close to the pile caps is deflected least, because the deflection is limited by the unmoving pile cap. This location therefore attracts more load than the locations further away from the pile cap and so the highest pressures are found alongside the pile cap, with the lowest pressures on the GR strip being found at the central point between the pile caps.

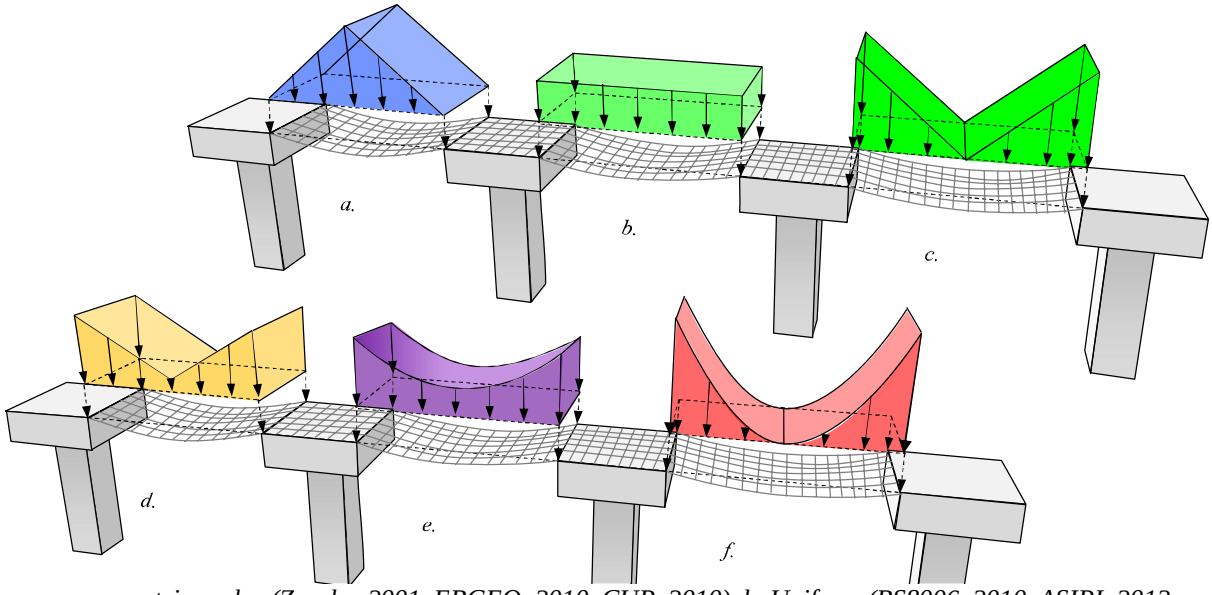

a. triangular (Zaeske, 2001, EBGEO, 2010, CUR, 2010), b. Uniform (BS8006, 2010, ASIRI, 2012, CUR, 2016 for the case with subsoil support), c. inverse-triangular (van Eekelen, 2012a and b, CUR226, 2016 for the case without or with limited subsoil support), d. inverse-triangular non-zero centre, e. parabolic non-zero centre, f. parabolic

Figure 7: Different load distributions on the GR strips

It is of importance to distinguish the situations with and without subsoil support.

If there is no subsoil support, the GR at the central point between the pile caps sags most and therefore attracts the least load. Van Eekelen et al. (2015) models the resulting load distribution with the inverse triangle (Figure 7*c*). This is a schematisation that represents reality: in reality, the load distribution may be different, probably with a value larger than zero in the centre, and probably the shape of the load distribution is not linear, but more like a cup-parabola. These alternatives are shown in Figure 7*d* to *f*.

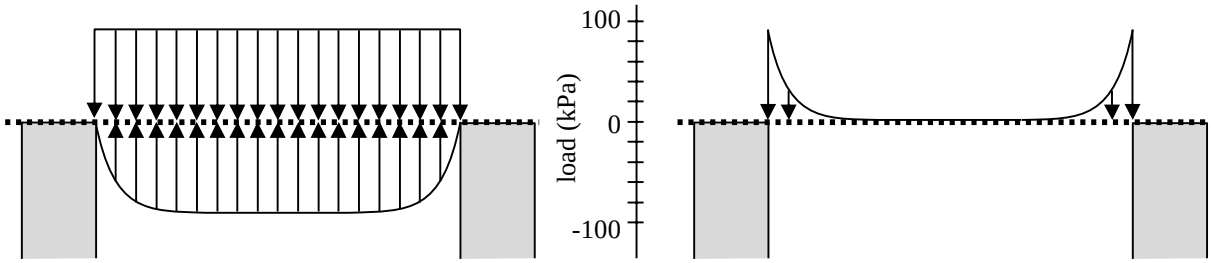

a. uniformly distributed load in combination with subsoil support *b. resulting net load distribution.*

Figure 8: uniform load distribution in the case of considerable subsoil support, analytical calculation of Van Eekelen et al. (2015) that simulates and agrees well with the field measurements of Briançon and Simon (2012).

If there is considerable subsoil support, the GR at the central point will sag less, and the GR sags more evenly, and the load will be distributed more uniformly. The uniform load (Figure 7*b*) is combined with the counter-pressure that is directed upwards, resulting in a *net* load distribution that matches a parabola-like load distribution as shown in Figure 8. Also in this case, the uniform load distribution is a schematisation that represents reality: in reality, the GR close to the pile cap may still attract more load than locations further away from the pile cap. And the shape of the load distribution will not be fully linear.

Question is: are the linear load descriptions of the load distribution sufficiently adequate? To answer this question, Figure 9 compares the relationship between a number of load distribution schematisations on the GR deflection and the maximum GR strain. For comparison reasons, the predictions of EBGEO and CUR (2010) have been included.

Figure 9*a* shows the situation without subsoil support. The figure shows that the more load is present at the central point, the more the GR sags. The blue triangular load therefore has the largest GR deflection at the central point. More load close to the pile caps, results in more deflection close to the pile cap, and less at the central point. The difference between the blue triangular load and the red parabola is considerable. Note that the difference between the pink inverse triangle and its yellow and purple variations is limited: these three give nearly the same GR deflection and maximum GR strain.

Figure 9*b* and *c* show the situation with subsoil support, with a subgrade reaction k = 100 and 200 kN/m^3. The figures show that the calculations with the inverse triangular or parabolic load distributions give more GR deflection close to the piles than at the central point. The resulting shape of the deformed GR leads to a relatively high GR strain. This is caused by the large counter-pressure in the centre of the GR strip, while the downward load midway between the piles is zero. This mechanism may occur in practice to a small extent, as shown by the measurements of Briançon and Simon (2012). However, stiffer subsoil leads to a more uniform load distribution as explained before (green in Figure 7 and Figure 9). Note that the difference between the pink inverse triangle and its yellow and purple variations is limited, also for these cases with subsoil support. It can therefore be concluded that the relatively simple inverse triangular load distribution is adequate.

Parabola	$q(x) = \lvert a \cdot x^2 \rvert$ where $a = 4 \cdot (3 \cdot q_{av} + 2 \cdot q_{min}) / L^2$
Parabola no-zero center	$q(x) = \lvert a \cdot x^2 + b \rvert$ where $a = -4(q_{min} - 3 \cdot q_{av} - 2 \cdot q_{min}) / L^2$ and $b = q_{min} = 0.25 \cdot q_{av}$
Inverse triangle	$q(x) = \lvert 4 q_{av} \cdot x / L \rvert$
Inverse triangle non-zero centre	$q(x) = \lvert 2(q_{max} - q_{min}) \cdot x / L + q_{min} \rvert$ where $q_{min} = 0.25 \cdot q_{av}$ and $q_{max} = 2 \cdot q_{av} - q_{min}$
Uniform	$q(x) = q_{av}$
Triangle	$q(x) = \lvert 4 q_{av} \cdot x / L \rvert^*$

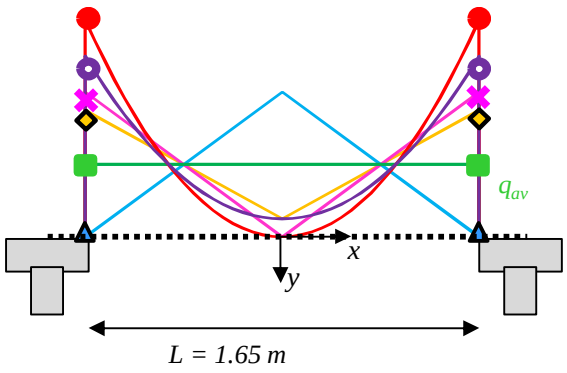

3

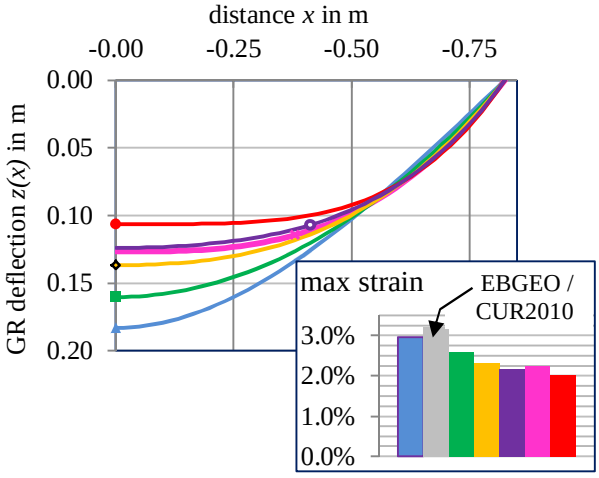

a. no subsoil: subgrade reaction k = 0 kN/m^3

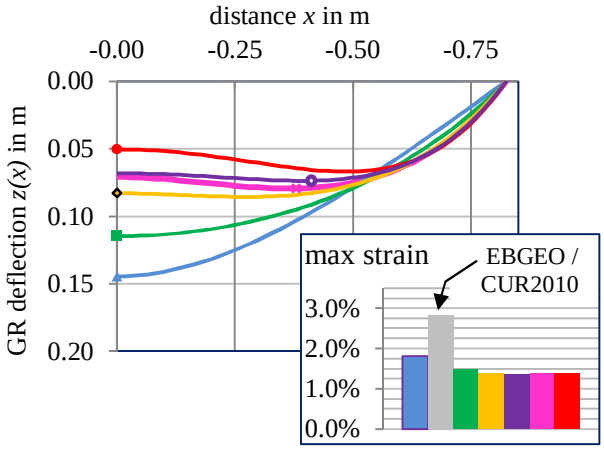

b. subgrade reaction k = 100 kN/m^3

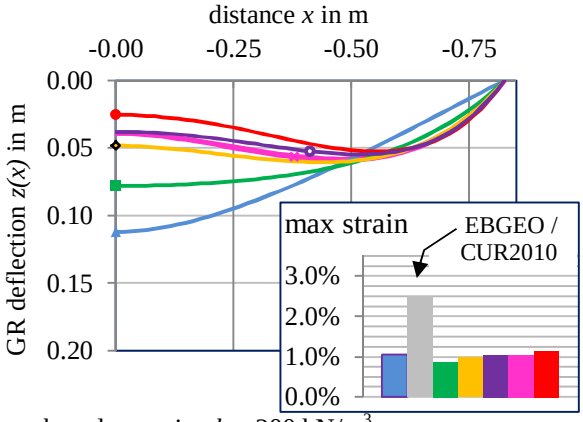

c. subgrade reaction k = 200 kN/m^3

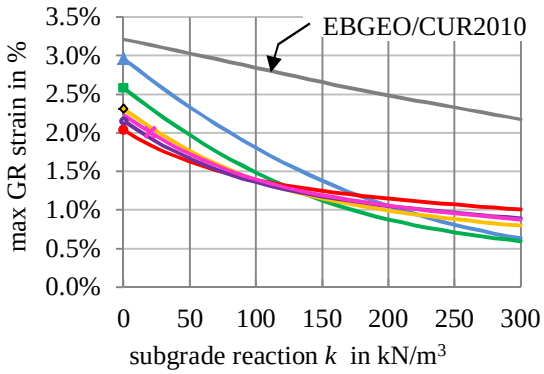

d. influence subgrade reaction on max GR strain

Figure 9: Influence of load distribution and subgrade reaction on GR deflection and GR strain. Input parameters given in Table 1, with square pile pattern $s_x = s_y$ = 2.00 m. Arching model (calculation step 1): Concentric Arches model of Van Eekelen et al., 2015 (CUR226, 2016) with result: $B+C$=65 kN/pile and q_{av} = 57 kPa. Additionally, the GR strain calculated with EBGEO/CUR2010 (Zaeske 2001) is given, in this case, $B+C$=76 kN/pile. Table modified after van Eekelen (2015)
* first half of span, with y-axis on pile cap edge

For the cases with subsoil support, the difference between Zaeske (2001), adopted in EBGEO/CUR226 (2010) and the other calculations using the Concentric Arches model is larger than for the case without subsoil; Zaeske's model gives a much higher GR strain than all CA calculations. This is because Zaeske (2001) only considers the subsoil beneath the GR strip under consideration between adjacent piles. The Concentric Arches model adopted the suggestions of Lodder et al. (2012) and Van Eekelen et al., (2012b), to use a modified value for the subgrade reaction *k* to take into account all subsoil underneath the entire GR. This suggestion is also in line with the work of Jones et al. (2010), Halvordson et al. (2010), Plaut et al. (2010) and Filz et al. (2012).

Van Eekelen et al. (2015) showed that the GR strain calculated with Zaeske's model is on average 2.5 times the GR strain measured in 7 field tests and 4 series of experiments. For the case that there is no subsoil support, or almost no subsoil support, the inverse triangular load distribution (Figure 7c) on the GR strips gives the best match with measurements in seven field studies and four series of experiments. When there is significant subsoil support, the uniform load distribution gives the best match.

The pragmatic approach proposed by Van Eekelen et al. (2015) and adopted in the CUR226 (2016) design guideline uses the Concentric Arches model in combination with subsoil support and the load distribution that gives the lowest GR strain. In this way, the inverse triangular distribution is applicable to the cases without, or with limited, subsoil support; a uniformly distributed load is applicable to the cases with substantial subsoil support. The GR strain calculated with the new model with this pragmatic approach is on average 1.1 times the measured GR strain. The calculated GR strain is therefore almost a perfect match with the measured GR strain.

6 CONCLUSIONS

If the piles are installed in a non-square rectangular pattern, a design made with the Concentric Arches model (van Eekelen et al, 2015, adopted in CUR226, 2016) has more reinforcement in the direction with the larger pile spacing. This is different for a design made with the Zaeske model (2001, adopted in EBGEO, 2010 and CUR226, 2010). Without subsoil support the Zaeske model gives the same reinforcement in both directions. With subsoil support Zaeske gives less reinforcement in the direction with the largest pile spacing. This is not realistic. This paper describes how the load distribution on the transverse and longitudinal GR strips of the two models explains the difference. Measurements or numerical calculations should be carried out to further study the load distribution in reinforced embankments on non-square rectangular pile patterns.

The Concentric Arches model models the resulting load distribution with the inverse triangle for the situation without subsoil support and uniform for the situation with subsoil support. This is a schematisation that represents reality: in reality, the load distribution may be different: parabolic and without a zero centre. The GR deflection and GR strains of several of these load distributions have been compared in this paper. It is concluded that there is not a large difference between the inverse triangular load distribution and alternative load distributions such as parabolic or inverse triangular without a 'zero-load' in the centre point. It can therefore be concluded that the relatively simple inverse triangular load distribution is adequate.

REFERENCES

ASIRI, 2012. Recommandations pour la conception, le dimensionnement, l'exécution et le contrôle de l'amélioration des sols de fondation par inclusions rigides, ISBN: 978-2-85978-462-1.

Briançon, L., Simon, B., 2012. Performance of Pile-Supported Embankment over Soft Soil: Full-Scale Experiment, *J. Geotechn. Geoenviron. Eng.* 2012. **138**:551-561.

BS8006-1: 2010. Code of practice for strengthened/reinforced soils and other fills. *British Standards Institution*, ISBN 978-0-580-53842-1.

CUR 226, 2010. Ontwerprichtlijn paalmatrassystemen (Design Guideline Piled Embankments, in Dutch). *Stichting CUR, Gou*da, ISBN 978-90-376-0518-1.

CUR 226, 2016. S.J.M van Eekelen and M.H.A. Brugman, Eds. Design Guideline Basal Reinforced Piled Embankments. *SBRCURnet & CRC Press*, ISBN 9789053676240, https://www.crcpress.com/Design-Guideline-Basal-Reinforced-Piled-Embankments/Eekelen-Brugman/9789053676240.

EBGEO, 2010. Empfehlungen für den Entwurf und die Berechnung von Erdkörpern mit Bewehrungen aus Geokunststoffen, Deutsche Gesellschaft für Geotechnik e.V. (DGGT).

Filz, G., Sloan, J., McGuire, M., Collin, J., Smith, M., 2012. Column-Supported Embankments: Settlement and Load Transfer. *Geotechnical Engineering State of the Art and Practice*: 54-77. doi: 10.1061/9780784412138.0003.

Halvordson, K.A., Plaut, R.H., Filz, G.M., 2010. Analysis of geosynthetic reinforcement in pile-supported embankments. Part II: 3D cable-net model. *Geosynthetics International* **17** (2), 68 - 76. ISSN: 1072-6349, E-ISSN: 1751-7613.

Jones, B.M., Plaut, R.H., Filz, G.M., 2010. Analysis of geosynthetic reinforcement in pile-supported embankments. Part I: 3D plate model. *Geosynthetics International* **17** (2), 59e67. ISSN: 1072-6349, E-ISSN: 1751-7613.

Lodder, H.J., van Eekelen, S.J.M., Bezuijen, A., 2012. The influence of subsoil reaction in a basal reinforced piled embankment. In: *Proceedings of Eurogeo5*, Valencia. Volume 5.

Plaut, R.H., Filz, G.M., 2010. Analysis of geosynthetic reinforcement in pilesupported embankments. Part III: axisymmetric model. *Geosynthetics International* **17** (2), 77-85. ISSN: 1072-6349, E-ISSN: 1751-7613.

Van der Peet, T.C., van Eekelen, S.J.M., 2014. 3D numerical analysis of basal reinforced piled embankments. In: *Proceedings of IGS10, September 2014, Berlin, Germany*. Paper no. 112.

Van Eekelen, S.J.M., Bezuijen, A., Lodder, H.J., van Tol, A.F., 2012a. Model experiments on piled embankments Part I. *Geotextiles and Geomembranes* **32**: 69 - 81.

Van Eekelen, S.J.M., Bezuijen, A., Lodder, H.J., van Tol, A.F., 2012b. Model experiments on piled embankments. Part II. *Geotextiles and Geomembranes* **32**: 82 – 94.

Van Eekelen, S.J.M., Bezuijen, A., Van Tol, A.F., 2013. An analytical model for arching in piled embankments. *Geotextiles and Geomembranes* **39**: 78 – 102.

Van Eekelen, S.J.M., 2015. Basal Reinforced Piled Embankments. *PhD thesis Technical University of Delft, Netherlands.* ISBN 978-94-6203-825-7 (print), ISBN 978-94-6203-826-4 (electronic version). Downloadable at: www.paalmatrassen.nl of www.piledembankments.com, incl. an excel file with the calculation model.

Van Eekelen, S.J.M., Bezuijen, A. van Tol, A.F., 2015. Validation of analytical models for the design of basal reinforced piled embankments. *Geotextiles and Geomembranes.* **43**, No. 1, 56 - 81.

Zaeske, D., 2001. Zur Wirkungsweise von unbewehrten und bewehrten mineralischen Tragschichten über pfahlartigen Gründungselementen. *Schriftenreihe Geotechnik, Uni Kassel*, Heft 10. ISBN 3-89792-048-4.